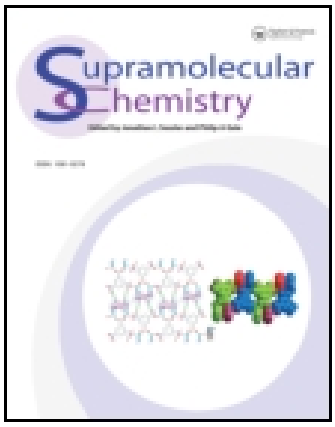

Supramolecular Chemistry
Publication details, including instructions for authors and subscription information:
http://www.tandfonline.com/loi/gsch20

Three coordination polymers of 5-aminoisophthalic acid with similar benzimidazole derivative ligands: synthesis, structure and DNA-binding studies

Yan Yang [a b], Liu-Ting Yan [b], Xu-Jian Luo [a], Rong-Huan Qin [a] & Wen-Gui Duan [b]
[a] School of Chemistry and Material, Yulin Normal University, Yulin, 537000, P.R. China
[b] School of Chemistry and Chemical Engineering, Guangxi University, Nanning, 530004, P.R. China
Published online: 25 Sep 2012.

To cite this article: Yan Yang, Liu-Ting Yan, Xu-Jian Luo, Rong-Huan Qin & Wen-Gui Duan (2012) Three coordination polymers of 5-aminoisophthalic acid with similar benzimidazole derivative ligands: synthesis, structure and DNA-binding studies, Supramolecular Chemistry, 24:11, 810-818, DOI: 10.1080/10610278.2012.720021

To link to this article: http://dx.doi.org/10.1080/10610278.2012.720021

Supramolecular Chemistry
Vol. 24, No. 11, November 2012, 810–818

Three coordination polymers of 5-aminoisophthalic acid with similar benzimidazole derivative ligands: synthesis, structure and DNA-binding studies

Yan Yang[a,b]*, Liu-Ting Yan[b], Xu-Jian Luo[a], Rong-Huan Qin[a] and Wen-Gui Duan[b]

[a]*School of Chemistry and Material, Yulin Normal University, Yulin 537000, P.R. China;* [b]*School of Chemistry and Chemical Engineering, Guangxi University, Nanning 530004, P.R. China*

(*Received 9 July 2012; final version received 7 August 2012*)

Three novel coordination polymers, $[Co(NH_2\text{-Aip})(H_2Bibim)]_n$ (**1**), $[Co(NH_2\text{-Aip})(HBibimop)]_n \cdot nH_2O$ (**2**) and $[Mn(NH_2\text{-Aip}) \cdot H_2O]_n \cdot 2nH_2O$ (**3**) with NH_2-Aip and similar benzimidazole derivative ligands (NH_2-Aip = 5-aminoisophthalic acid, H_2Bibim = 2,2′-bibenzimidazole and HBibimop = 1,3-bis(benzimidazol-2-yl)-2-oxapropane), have been synthesised under hydrothermal conditions and structurally characterised by single-crystal X-ray diffraction analysis, elemental analysis and IR spectroscopy. 5-Aminoisophthalic acid ligand adopts μ_2-, μ_3- and μ_4-bridge coordination fashion and benzimidazole derivatives exist as terminal- and bridge-mode in complexes **1**–**3**. The intricate hydrogen bonds and $\pi-\pi$ stacking interactions in supramolecular framework are discussed. Using the combination of ultraviolet–visible absorption titration and fluorescence spectra, the experimental results show that complexes **1** and **2** bind to DNA in an intercalative mode and their DNA-binding constants (K_b) are also found.

Keywords: crystal structure; mixed ligand; fluorescence; DNA-binding studies

Introduction

In recent years, many anticancer drugs have been found to exert their biological activities by interacting with DNA (*1*). Therefore, the drug–DNA interaction has been extensively studied for their potential application in understanding the molecular mechanisms of drug actions and designing specific DNA-targeted drugs. Many drugs bind to DNA mainly through intercalation, groove-binding and covalent linkages (*2*). These interactions may make changes in the structure of DNA to inhibit DNA duplication and cancer cell cleavage. As the functional groups of the active sites of a number of enzymes, benzimidazoles can participate in many important biochemical reactions (*3*), benzimidazole derivatives contain multiple nitrogen donor sites with the possibility of reversible protonation and deprotonation properties and can be coordinated to transition metals by elaborating tunable coordination modes (Chart 1), which have been utilised in coordination polymer for the preparation of different networks (*4*) through intermolecular hydrogen bonds (*5–8*) and $\pi-\pi$ stacking interactions (*9–12*). On the other hand, as a rigid and versatile bridging ligand, 5-aminoisophthalic acid has been extensively studied for designing new coordination polymer because its two carboxylic groups can bond to metal centres and the amino group coexisting in isophthalic acid with lone pair electrons situated in sp^3 hybrid orbital can not only act as a hydrogen bond acceptor, but can also be coordinated to transition metals (Chart 1) (*13–17*). We have reported some complexes (*18–20*) in the last several years.

In this context, we synthesised three novel coordination polymers of $[Co(NH_2\text{-Aip})(H_2Bibim)]_n$ (**1**), $[Co(NH_2\text{-Aip})(HBibimop)]_n \cdot nH_2O$ (**2**) and $[Mn(NH_2\text{-Aip}) \cdot H_2O]_n \cdot 2nH_2O$ (**3**) with NH_2-Aip and similar benzimidazole derivative ligands (NH_2-Aip = 5-aminoisophthalic acid, H_2Bibim = 2,2′-bibenzimidazole and HBibimop = 1,3-bis(benzimidazol-2-yl)-2-oxapropane), in which both ligands can be coordinated to cobalt or manganese ions with terminal- and bridge-mode (Chart 1). Ultraviolet–visible (UV–vis) absorption titration and fluorescence spectra methods have been used for the study of the interaction of complex with DNA.

Experimental

Materials and methods

Calf thymus DNA (ct-DNA) was purchased from the Sino-American Biotechnology Company. Other reagents were bought from commercial sources and used without further purification. IR spectra were recorded in the range of 4000–400 cm^{-1} on Perkin-Elmer Spectrum One FT/IR spectrometer using a KBr pellet. Elemental analysis (C, H and N) was performed on a Perkin-Elemer 2400II CHN elemental analyser. UV–vis absorption titration was performed on a Cary 100 Conc. UV–vis spectrophotometer. Fluorescence emission titration was performed on

*Corresponding author. Email: yy135175@163.com

ISSN 1061-0278 print/ISSN 1029-0478 online

http://dx.doi.org/10.1080/10610278.2012.720021
http://www.tandfonline.com

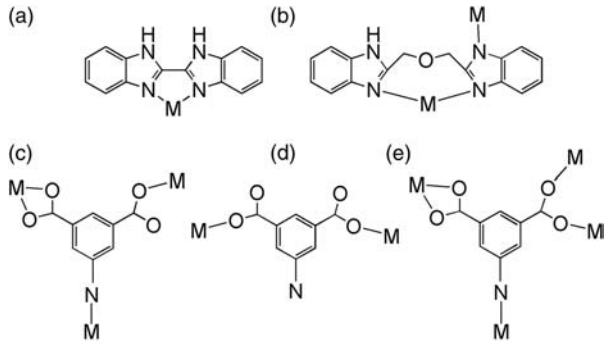

Chart 1. Coordination mode of the three ligands.

a Shimadzu RF-5301/PC spectrofluorometer. The crystal structure was determined by a Bruker APEX area-detector diffractometer and employing the SHELXTL crystallographic software. In DNA-binding studies, all complexes were dissolved in dimethyl sulfoxide (DMSO) for preparation of stock solution at 1.0×10^{-6} M. Buffer (5 mM tris(hydroxymethyl)aminomethane (Tris)-hydrochloride, 50 mM NaCl, pH 7.35) was used for UV absorption and emission titration experiments. The concentration of ct-DNA was determined spectrophotometrically assuming that molar absorption is 6600 $M^{-1}cm^{-1}$ (260 nm) (*21*, *22*). The UV absorption and emission titrations of complexes **1** and **2** in water/DMSO 10% in the presence of a buffer were performed by using a fixed complex concentration to which increments of the DNA stock solution were added ([DNA]/[compound] ranged from 0 to 10). Complex–DNA solutions were allowed to incubate for 15 min before the UV absorption and emission spectra were recorded.

Synthesis of [Co(NH_2-Aip)(H_2Bibim)]$_n$ (1)

For the hydrothermal reaction of $CoCl_2$ (0.5 mmol), H_2Bibim (0.5 mmol), NH_2-Aip (0.5 mmol) and water (18 ml), the mixture was stirred for 10 min in air, then transferred and sealed into a 23-ml Teflon reactor, which was heated at 160°C for 5 days and then cooled to room temperature. Red block crystals were obtained (yield 23% based on NH_2-Aip), filtered off, washed with distilled water and dried in air. Elemental analysis (%): Anal. Calcd. C, 55.93; H, 3.18; N, 14.83; found C, 55.78; H, 3.24; N, 14.79. IR (KBr pellets, cm^{-1}): $\nu = 3022$, 2955, 1622, 1569, 1531, 1454, 1428, 1390, 1319, 1266, 1246, 1179, 1159, 1080, 1043, 1005, 931, 918, 788, 695.

Synthesis of [Co(NH_2-Aip)(HBibimop)]$_n \cdot n H_2O$ (2)

For the hydrothermal reaction of $Co(NO_3)_2 \cdot 6H_2O$ (0.5 mmol), HBibimop (0.25 mmol), NH_2-Aip (0.25 mmol) and water (15 ml), the mixture was stirred for 20 min in air, then transferred and sealed into a 23 ml Teflon reactor, which was heated at 110°C for 4 days and then cooled to room temperature. Red needle-shaped crystals were obtained (yield 48% based on Co), filtered off, washed with distilled water and dried in air. Elemental analysis (%): Anal. Calcd. C, 54.06; H, 4.08; N, 14.18; found C, 54.03; H, 4.09; N, 14.17. IR (KBr pellets, cm^{-1}): $\nu = 3058$, 1559, 1427, 1375, 1329, 1268, 1121, 1049, 999, 958, 920, 850, 783, 757, 733.

Synthesis of [Mn(NH_2-Aip)$\cdot H_2O$]$_n \cdot 2nH_2O$ (3)

For the hydrothermal reaction of $MnSO_4$ (1 mmol), NH_2-Aip (0.5 mmol) and water (15 ml), the mixture was stirred for 30 min in air, then transferred and sealed into a 23 ml Teflon reactor, which was heated at 160°C for 5 days and then cooled to room temperature. Colourless crystals were obtained (yield 63% based on NH_2-Aip), filtered off, washed with distilled water and dried in air. Elemental analysis (%): Anal. Calcd. C, 33.45; H, 3.48; N, 4.88; found C, 33.51; H, 3.53; N, 4.83. IR (KBr pellets, cm^{-1}): $\nu = 3093$, 1690, 1624, 1588, 1550, 1451, 1402, 1291, 1256, 1223, 1111, 908, 751, 683, 592.

X-ray crystallography

Diffraction data were collected on a Bruker Smart Apex CZN diffractometer with graphite-monochromated Mo$K\alpha$ radiation ($\lambda = 0.71073$ Å) at 296 K. Absorption correction was applied by SADABS (*23*). The structure was solved by Direct Methods and refined with full-matrix least-squares technique using SHELXTL (*24*). All non-hydrogen atoms were refined with anisotropic displacement parameters. Crystal data, details of the data collection and refinement are summarised in Table 1, and selected bond lengths and angles are presented in Table 2; the hydrogen bond lengths (Å) and bond angles (deg) are listed in Table 3.

Crystal structures of complexes 1–3

Single-crystal X-ray diffraction analysis reveals that compound **1** has a supramolecular framework structure formed by one-dimensional (1D) bi-chain and crystallises in the monoclinic P21/*n* space group. Asymmetric unit contains one Co(II) atom, one H_2Bibim ligand and one Aip ligand (Aip = 5-aminoisophthalic acid) (Figure 1). The distorted octahedral Co(II) atom geometry (Scheme 1(a)) is established by three oxygen atoms (O1a, O2a and O4b) and one nitrogen atom (N5c) from three different Aip ligands and two nitrogen atoms (N1a and N3a) from one H_2Bibim ligand. The basal plane consists of four almost coplanar atoms (O1a, O2a, O4b and N3a), and the N1a and N5c atoms occupy the apical positions (Figure 1(a)). The Co—O distances are in the range of 2.012(3)–2.209(4) Å, and the Co—N distances are in the range of 2.105(4)–2.270(4) Å

Table 1. Crystal data and structure refinement for complexes **1**–**3**.

Identification code	**1**	**2**	**3**
Empirical formula	$C_{22}H_{15}CoN_5O_4$	$C_{40}H_{36}Co_2N_9O_8$	$C_8H_{10}MnN_1O_7$
Formula weight	472.32	888.64	288.12
Temp (K)	296(2)	296(2)	293(2)
Crystal system	Monoclinic	Monoclinic	Triclinic
Space group	P21/*n*	C2/*c*	P-1
a (Å)	12.605(5)	26.209(3)	7.7732(16)
b (Å)	8.774(3)	9.6927(12)	8.6392(17)
c (Å)	16.706(6)	19.143(4)	8.7331(17)
α (deg)	90.00	90.00	85.45(3)
β (deg)	98.571(5)	130.19(10)	76.06(3)
γ (deg)	90.00	90.00	66.56(3)
V (Å^3)	1827.0(12)	3714.9(10)	522.14(18)
Cryst size (mm)	0.36 × 0.30 × 0.20	0.30 × 0.26 × 0.22	0.26 × 0.20 × 0.18
Z	17	4	7
D_c (g cm^{-3})	1.710	1.589	1.826
μ (mm^{-1})	0.985	0.962	1.289
F(000)	956	1828	292
Limiting indices	$-14 \le h \le 14$	$-31 \le h \le 31$	$-10 \le h \le 10$
	$-10 \le k \le 10$	$-10 \le k \le 11$	$-11 \le k \le 11$
	$-16 \le l \le 19$	$-22 \le l \le 22$	$-11 \le l \le 11$
Reflections	9304	10132	5492
Independent	3204	3279	2373
Observed data	2398	2490	2178
Npar	289	268	178
R_{int}	0.1276	0.0401	0.0187
GOF	1.067	1.021	1.166
R_1[a] ($I > 2\sigma(I)$)	0.0742	0.0428	0.0290
wR_2[b] (all data)	0.2180	0.1137	0.0716
Max/min electron density (eÅ^{-3})	1.046/−0.990	0.657/−0.606	0.380/−0.293
Theta range (°)	0.993, 25.01	0.997, 25.01	0.994, 27.44

[a] $R_1 = \sum||F_o| - |F_c||/\sum|F_o|$.

[b] $wR_2 = [\sum w(F_o^2 - F_c^2)^2/\sum w(F_o^2)^2]^{1/2}$.

Table 2. Selected bond lengths (Å) and bond angles (°) for complexes **1**–**3**.

Complex **1**		Complex **2**		Complex **3**	
Co1—O1	2.127(4)	Co1—O1	2.022(2)	Mn1—O1	2.2459(15)
Co1—O2	2.209(4)	Co1—N2	2.045(3)	Mn1—O2	2.3519(16)
Co1—O4a	2.012(3)	Co1—N4	2.030(3)	Mn1—O3	2.1189(17)
Co1—N1	2.179(4)	Co1—N5	2.041(3)	Mn1—O4	2.1438(16)
Co1—N3	2.105(4)			Mn1—O5	2.1574(16)
Co1—N5b	2.270(4)			Mn1—N1	2.3816(19)
O1—Co1—O2	60.40(12)	O1—Co1—N2	101.38(11)	O1—Mn1—O2	57.12(5)
O1—Co1—N1	92.60(15)	O1—Co1—N4	109.19(11)	O1—Mn1—N1	94.33(6)
O1—Co1—N5b	84.87(15)	O1—Co1—N5	96.97(10)	O2—Mn1—N1	85.91(6)
O2—Co1—N5b	90.03(14)	N4—Co1—N2	124.37(11)	O3—Mn1—O1	90.59(6)
O4a—Co1—O1	95.33(14)	N4—Co1—N5	110.82(11)	O3—Mn1—O2	145.81(5)
O4a—Co1—O2	155.67(14)	N5—Co1—N2	110.13(11)	O3—Mn1—O4	100.30(6)
O4a—Co1—N1	98.09(15)			O3—Mn1—O5	120.90(7)
O4a—Co1—N3	99.71(16)			O3—Mn1—N1	85.74(6)
O4a—Co1—N5b	85.72(14)			O4—Mn1—O1	89.97(6)
N1—Co1—O2	85.62(15)			O4—Mn1—O2	91.34(6)
N1—Co1—N5b	175.62(16)			O4—Mn1—O5	89.51(7)
N3—Co1—O1	163.51(15)			O4—Mn1—N1	172.56(5)
N3—Co1—O2	104.58(15)			O5—Mn1—O1	148.04(6)
N3—Co1—N1	78.70(16)			O5—Mn1—O2	90.95(7)
N3—Co1—N5b	102.86(16)			O5—Mn1—N1	83.63(7)

Note: Symmetry transformations used to generate equivalent atoms: Complex **1**, a = $-x+2, -y+2, -z+2$; b = $-x+2, -y+1, -z+2$.

Table 3. Distances (Å) and angles (°) of hydrogen bonds for complexes **1**–**3**.

D—H···A	*d*(D—H)	*d*(H···A)	*d*(D···A)	<(D—H···A)
Complex **1**				
N2—H2···O3	0.8600	2.0500	2.853	155.03 ($x-1, y, z$)
N4—H4···O3	0.8600	2.0520	2.860	156.30 ($x-1, y, z$)
N5—H5A···O3	0.9000	2.3820	3.173	146.60 ($-x+5/2, y-1/2, -z+3/2$)
Complex **2**				
N1—H1B···O4	0.8900	2.3900	3.029(8)	128.40 ($x, y-1, z$)
N1—H1C···O4	0.8900	2.3200	3.029(8)	136.40 ($-x, y-1, -z+1/2$)
N3—H3···O2	0.8600	1.9800	2.696(4)	140.60 ($-x, -y+1, -z$)
Complex **3**				
O5—H5A···O2	0.7970	1.9330	2.721	169.66 ($-x+1, -y, -z$)
O5—H5B···O6	0.8360	1.9390	2.758	165.77 ($-x+1, -y, -z+1$)
O6—H6A···O1	0.8500	2.0440	2.834	154.32 ($-x+1, -y+1, -z+1$)
O6—H6B···O6	0.8500	2.1850	2.894	140.78 ($-x+1, -y+1, -z+1$)
O7—H7A···O6	0.8500	2.0470	2.867	161.90
O7—H7B···O4	0.8500	2.0760	2.863	153.71
N1—H1B···O7	0.9000	2.2030	3.033	152.90 ($x-1, y, z$)

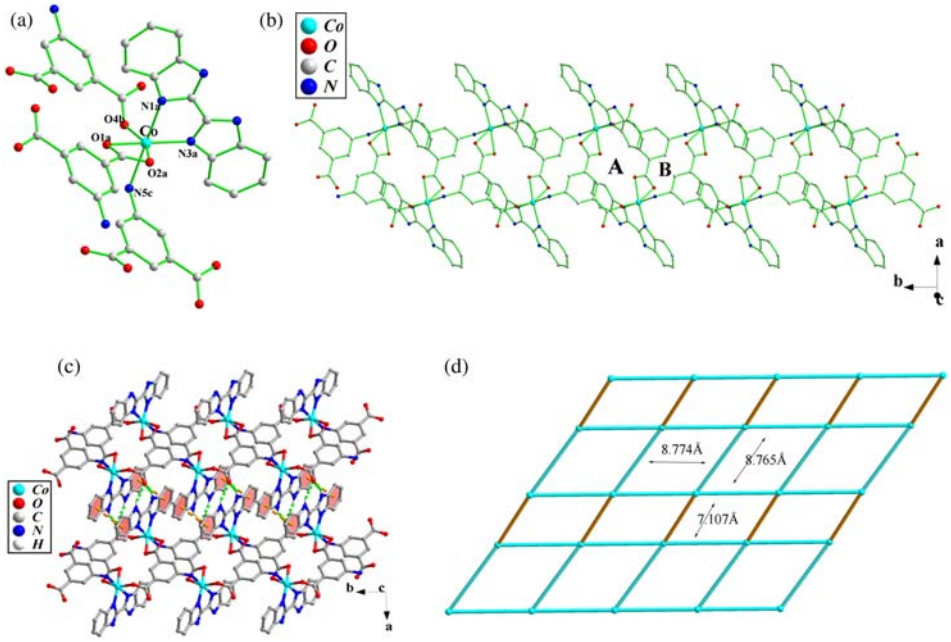

Figure 1. (a) Coordination environment of complex **1**; (b) 1D bi-chain of complex **1** with two different subrings A and B, hydrogen atoms are omitted for clarity. (c) $\pi-\pi$ Stacking and hydrogen-bonding interactions of complex **1**; (d) simplified (4, 4) topology structure of complex **1**, hydrogen atoms are omitted for clarity.

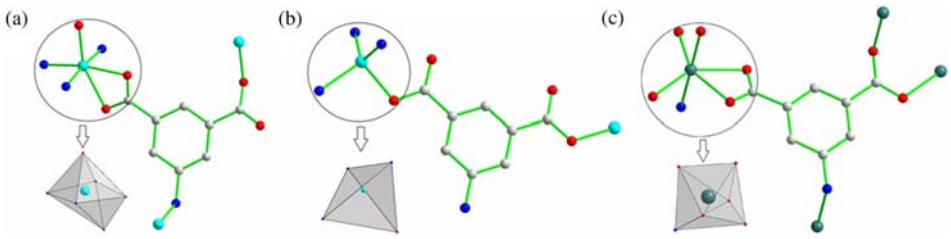

Scheme 1. (a) Coordination mode of Aip and the coordination sphere of the Co(II) ion in complex **1**. (b) Coordination mode of Aip and coordination sphere of the Co(II) ion in complex **2**. (c) Coordination mode of Aip and coordination sphere of the Mn(II) ion in complex **3**.

(Table 2), respectively. In the structure, the Aip ligand adopts (μ_3 – ((η^2 – O_1, O_2), O_3, N_1)) bridging coordination fashion (Chart 1(c)): one carboxylate group adopts mono-bisdentate coordination mode to chelate two Co(II) centres, and another carboxylate group and amino group act as monodentate ligands. The adjacent Co(II) atoms are connected by μ_3-bridged Aip into 1D bi-chain structure along the *b* direction, while the H_2Bibim ligand acts as a chelating ligand (Chart 1(a)) and alternately arranges at the sides of the chains in an outward fashion (Figure 1(b)). The most interesting feature for polymer **1** is that the Aip ligands link Co(II) centres in different ways to produce two different subrings A and B, which are 16-membered (A rings) and 14-membered rings (B rings) (Figure 1(b)). It should be noted that there are three types of hydrogen bonds in this structure: the uncoordinated O atoms of Aip ligands act as hydrogen-bonding acceptors to form hydrogen bonds with the uncoordinated imidazole N atoms of H_2Bibim ligands and amino-group nitrogen atoms of Aip ligands, N2—H2···O3, N4—H4···O3 and N5-H5A···O3 with the distances (*d*(D···A)) being 2.853, 2.860 and 3.173 Å, and O—H···N angles being 155.03, 156.30 and 146.60° (Table 3). At the same time, the face-to-face $\pi-\pi$ stacking interactions (the centroid···centroid separation is 3.696 Å) are also observed, as shown in Figure 1(c). The 1D bi-chains mentioned above are interconnected through these hydrogen bonds and $\pi-\pi$ stacking interactions between benzene rings of the adjacent H_2Bibim groups to result in a layer structure in the *ab* plane (Figure 1(c)) and further stabilise the supramolecular network. This layer can be reduced to a (4, 4) topology (Figure 1(d)).

Single-crystal X-ray diffraction analysis shows that compound **2** is a two-dimensional (2D) structure in which there are one Co(II) atom, moiety bis-monodentate Aip ligand, one HBibimop ligand and one lattice water molecule in each independent crystallographic unit (Figure 2(a)). Each Co(II) atom in **2** is primarily four-coordinated by one carboxylate oxygen atom of one Aip ligand (Co1—O1 = 2.022(2) Å) and three nitrogen atoms from HBibimop ligand (Co—N = 2.030(3)–2.045(3) Å, Table 2, the average value is 2.039 Å) to furnish a distorted trigonal pyramid geometry (Figure 2(a) and Scheme 1(b)). Different from **1**, Aip ligand adopts bis-monodentate bridging mode (Chart 1(d)) to connect Co(II) atoms to form 1D undulate chain along the *a* axis (Figure 2(b)). HBibimop ligand acts as chelating-bidentate and bridging-monodentate mode (Chart 1(b)) to link Co(II) atoms of neighbouring chains to produce an undulate 2D layer parallel to the *ab* plane through interchain Co—N bonds (Co1—N5 = 2.041(3) Å) (Figure 2(b)). So, Auxiliary HBibimop ligands in this 2D structure act actually as chelating-bidentate and bridging-monodentate mode in **2**, as shown in Chart 1(b). Up to date, the terminal-mode (μ_1-(η^2-N, N)) of HBibimop has been mostly reported (*25–27*); however, rare examples with bridge-mode (μ_2 – (η^2 – N, N), N) have been observed. In addition, there exist N1—H1B···O4 and N1—H1C···O4 hydrogen-bond interactions with their distances (*d*(D···A)) being 3.029(8) Å, and N—H···O angles being 128.40° and 136.40° (Figure 2(b) and Table 3) in the 2D structure of **2** which further stabilise the layer structure. Furthermore, strong interlayer N—H···O hydrogen-bond interactions with the separation (*d*(D···A)) being 2.696(4) Å and N—H···O angles being 140.60° also contribute to this 3D supramolecular structure (Figure 2(c)).

Single-crystal X-ray diffraction analysis indicates that compound **3** is a 2D supramolecular network structure in which asymmetric unit contains one Mn(II) atom, one Aip ligand, one coordinated water and two lattice water molecules (Figure 3(a)). Mn(II) is six-coordinated by four oxygen atoms from three distinct Aip ligands, one amino group nitrogen atom from one Aip ligand and one oxygen atom of aqueous molecule to form distorted octahedral geometry (Scheme 1(c)), as shown in Figure 3(a). Compared with complexes **1** and **2**, the Aip ligand adopts (μ_4 – (η^2 – O_1, O_2), O_3, O_4, *N*) mode (Chart 1(e)): one carboxylate group adopts mono-bidentate (*syn-syn*) coordination mode to bridge two Mn(II) atoms, another carboxylate group acts as a chelating bidentate ligand and its amino group uses bridging monodentate mode to join Mn(II) centres. The binuclear $Mn_2(CO_2)$ unit in compound **3** is bridged by four Aip ligands to result in the 2D layers parallel to the *bc* plane (Figure 3(b)) with four kinds of interlocking rings which are the 14-membered rings (A rings), the 16-membered rings (B rings), the 8-membered rings (C rings) and the 14-membered rings

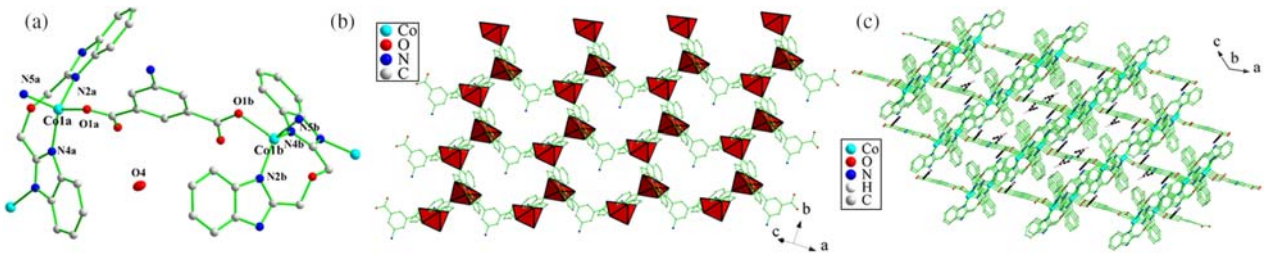

Figure 2. (a) Coordination environment of complex **2**, (b) the 2D layers of complex **2** and (c) the three-dimensional supramolecular network of complex **2**, hydrogen atoms are omitted for clarity.

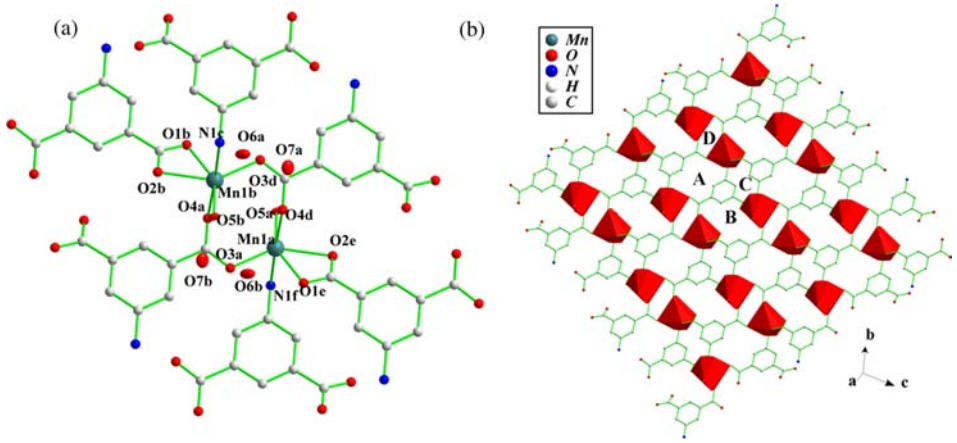

Figure 3. (a) Coordination environment of complex **3** and (b) the 2D layers of complex **3**, hydrogen atoms are omitted for clarity.

(D rings) with the Mn···Mn distances of 8.0008, 8.0693, 4.1435 and 8.0794 Å, respectively (Figure 3(b)). In the structure, there exist five types of hydrogen-bonding interactions: the oxygen atoms (O_5) of coordinated water act as hydrogen bond donors to form hydrogen bonds with the coordinated carboxylate oxygen atoms (O_2) of Aip ligands and the oxygen atoms (O_6) of lattice water, O5—H5A···O2 and O5—H5B···O6 with the separations (d(D···A)) being 2.721 and 2.758 Å, and O—H···O angles being 169.66° and 165.77° (Table 3); at the same time, the oxygen atoms (O_6 or O_7) of lattice water act as hydrogen bond donors to form hydrogen bonds with the coordinated carboxylate oxygen atoms (O_1 or O_4) and amino group N atoms of Aip ligands, O6—H6A···O1, O7—H7B···O4 and N1—H1B···O7 with the distances (d(D···A)) being 2.834, 2.863 and 3.033 Å, respectively, O—H···O angles being 154.32° and 153.71°, as well as O—H···N angles being 152.90° (Table 3). In addition, hydrogen bonds have been found between lattice waters, O6—H6B···O6 and O7—H7A···O6 with the separations (d(D···A)) being 2.894 and 2.867 Å, and O—H···O angles being 140.78° and 161.90° (Table 3).

DNA-binding studies

Absorption titrations

Figure 4 shows the UV–vis absorption spectra of complexes **1** and **2** in the presence of increasing concentrations of DNA. Complexes **1** and **2** represent the two absorption peaks at 241, 275 nm (Figure 4(a)) and at 277, 313 nm (Figure 4(b)), respectively, which can be assigned to the $\pi \rightarrow \pi^*$ (at 241 nm) and $n \rightarrow \pi^*$ (at 275, 277 and 313 nm) transitions of the benzimidazole rings. Such an observation is the result of the so-called 'additive effect' of absorption spectra which the metal atoms are simultaneously coordinated to two ligands, which are Aip ligands and H_2Bibim (for **1**) or HBibimop ligands (for **2**). With increasing concentrations of DNA added, significant hyperchromism, red-shift and blue-shift are observed. There are 93% hyperchromism with a 9-nm red-shift (from 241 to 250 nm) at 241 nm and 400% hyperchromism with an 8-nm blue-shift (from 275 to 267 nm) at 275 nm for **1**. Different from the peak absorption intensities of compound **1**, the peak absorption intensities of compound **2** only increase about 8% at 277 nm and do hardly change at 313 nm, but the observation of the red-shift or blue-shift

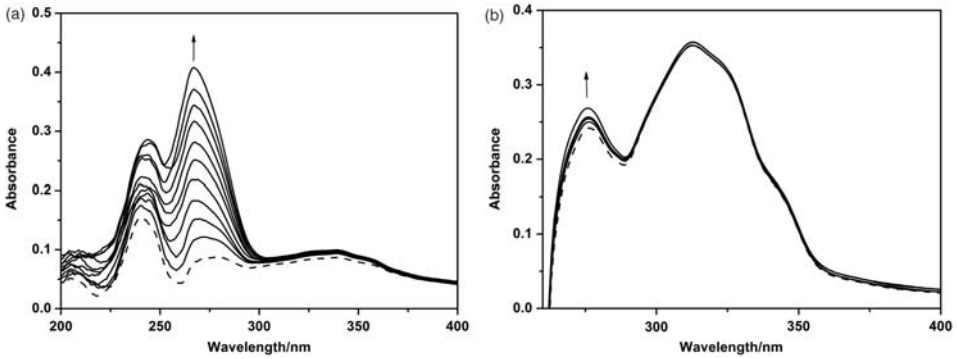

Figure 4. UV absorption spectra of complexes **1** and **2** with increasing concentration of DNA (concentration of complex is 1.0×10^{-6} M, [DNA]/[compound] ranged from 0 to 10).

has not been found. When the ratio of [DNA]/[Complex] increases from 0 to 10, the compound can insert the adenine base stacks of double-helical DNA, which causes hydrophobic interaction to be composed of base stacking strength and van der Waals force to vary correspondingly, affecting the stability of the conformation of DNA and making the double-helical structure of DNA cause damage which lead to unwinding of the double-helical structure and increasing in UV–vis absorption of purine and pyrimidine bases (*28*). However, hyperchromism is likely the result of the damaged hydrogen-bonding interactions between the complex aggregates and complex molecules (*29*, *30*) brought about by the penetration of complexes into the DNA base stacks. According to the literature (*31*–*34*), hyperchromism (or hypochromism) and bathochromism can be observed as the small molecule binds to double-strand DNA by classical intercalation mode. However, there is no obvious hypochromism or bathochromism when small molecule can interact with DNA via groove binding or electrostatic interaction. In brief, complex **1** can interact into the base pairs of double-helical DNA via an intercalative mode and complex **2** may bind to DNA via the combined mode of intercalation and groove binding.

To compare quantitatively the binding strength of the compounds, the intrinsic binding constants K_b with DNA are determined from the increase in the absorbance with increasing concentrations of DNA using the equation (*35*):

$$\frac{\mathrm{DNA}}{\varepsilon_a - \varepsilon_f} = \frac{\mathrm{DNA}}{\varepsilon_b - \varepsilon_f} + \frac{1}{[K_b(\varepsilon_b - \varepsilon_f)]},$$

where ε_a, ε_f and ε_b are the extinction coefficients of the complex at a given DNA concentration, the complex free in solution and the complex fully bound to DNA, respectively, K_b is the equilibrium binding constant, [DNA] is the DNA concentration in 0.1 M Tris buffer (pH 7.35) containing 10% DMSO. The intrinsic binding constants, K_b, of **1** and **2** for DNA are determined to be 2.99×10^5 and 4.05×10^5. In the plot of [DNA]/($\varepsilon_f - \varepsilon_a$) versus [DNA], the intrinsic binding constants, K_b, can be obtained by the ratio of the slope to intercept. Complex **2** displays larger binding constant than does complex **1** since the groove binding of complex **2** is much more intense than the intercalation of complex **1**.

Fluorescence studies

The fluorescence emission spectra of complexes **1** and **2** in the presence of increasing concentrations of DNA are shown in Figure 5. As shown in Figure 5(a), upon excitation using a wavelength of 326 nm, complex **1** displays luminescence with three emission maxima at 346, 364 and 382 nm, which can be assigned to the $\pi \rightarrow \pi^*$ transitions of the benzimidazole rings. Upon addition of DNA, the luminescence intensity is reduced compared with that of the parent $[Co(NH_2\text{-}Aip)(H_2Bibim)]_n$ in the absence of DNA under similar conditions, reaching a minimum at the ratio of [DNA]/[Complex **1**] = 10, at which there is a 0.88-, 0.91- and 0.92-fold decrease in the fluorescence intensity of complex **1** compared with that in the absence of DNA. The reduced luminescence observed for complex **1** in 0.1 M Tris buffer (pH 7.35) containing 10% DMSO can be rationalised, primarily, in terms of an intramolecular photoinduced electron-transfer quenching of its metal-to-ligand charge transfer (MLCT) state. The decreases in emission intensities of compound **1** most probably result from the interaction between the small molecules and DNA; since there are enrichment domains of A-T and C-G sequence in the base pairs of DNA sequence, fluorescence emission will give rise to change if the compound is intercalating the different orientation of the DNA bases. When the compound is intercalating into the C-G sequence, the easier electron transfer between the excited state and guanosine G can result in effective quenching of fluorescence because the distance between them is very close, that is 0.34 nm or so, and guanosine G has better electron donating ability (*36*, *37*). Furthermore, the fluorescence emission of the excited state in complex **1** is

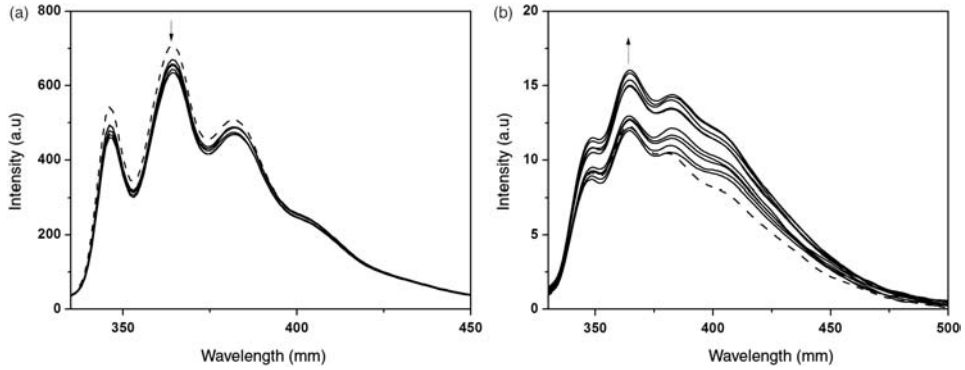

Figure 5. Emission spectra of complexes **1** and **2** in 0.1 M Tris buffer (pH 7.35) containing 10% DMSO in the absence (. . .) and presence (—) of DNA.

probably quenched due to proton transfer from the solvents to the benzimidazole rings (*38*). The decreases in fluorescence emission also suggest that compound **1** interacts with DNA strongly. As shown in Figure 5(b), complex **2** exhibits three fluorescent emission bands at 346, 365 and 381 nm upon being excited at 312 nm, which is predominantly $\pi \rightarrow \pi^*$ transition fluorescence. As opposed to the fluorescence emission of complex **1**, the fluorescence emission for complex **2** increases with increasing amounts of DNA. When the ratio [DNA]/[Complex **2**] = 10, the 1.35-, 1.33- and 1.42-fold increase in the fluorescence intensity of complex **2** has been found compared with that in the absence of double-helical DNA for **2**. This observation suggests that complex **2** binds to DNA by an intercalative mode. The strong binding of complex **2** to DNA can give rise to the so-called 'molecular light switch effect', in which the nearly undetectable emission from the MLCT excited state in water becomes strongly enhanced upon binding (*34*). This is mostly because of the intercalation of complex **2** into the base pairs of DNA, which is hydrophobic inside the helix, limits the collision and energy dissipation with the environmental water and oxygen (*39–41*). As far as compound **2** is concerned, the weak fluorescence is the result of increasing the loss of energy via non-radiative decay of the intraligand excited state, which was suggested to be highly quenched by lattice aqueous in compound **2** due to proton transfer from the solvent to the benzimidazole ligand (*42–45*).

Summary

In summary, we successfully synthesised three novel coordination polymers based on 5-aminoisophthalic acid and similar benzimidazole derivative ligands with different metals by hydrothermal method. The intricate hydrogen bonding and $\pi-\pi$ stacking interactions in supramolecular framework were discussed. In addition, we have attempted to unravel the DNA interactions of complexes **1** and **2** in this study. Furthermore, UV–vis absorption titration and fluorescence spectra methods have been used for the study of the interaction of complexes with DNA. The results have shown that the corresponding fluorescence intensities increase for complex **2** and decrease for complex **1**, and significant hyperchromism, red-shift and blue-shift are observed in UV–vis absorption spectra with increasing concentrations of DNA. The DNA-binding constants of complexes **1** and **2** have also been found. All of the results have demonstrated that there exists stronger intercalation of complexes into the base pairs of double-helical DNA.

Supplementary materials

CCDC nos 841894 (**1**), 885798 (**2**) and 851817 (**3**), contain the supplementary crystallographic data. These data can be obtained via the Cambridge Crystallographic Data Centre (deposit@ccdc.cam.ac.uk; http://www.ccdc.cam.ac.uk/deposit).

Acknowledgements

We acknowledge financial support by the National Natural Science Foundation of China (No. 51062016) and the Project of Science Research & Technology Exploitation of Guangxi Province (No. 11107013-8).

References

(1) Altinok, A.; Lévi, F.; Goldbeter, A.; Eur *J. Pharm. Sci.* **2009**, *36*, 20–38.
(2) Edrem, A.; Ozsoz, M. *Electroanalytical* **2009**, *14*, 965–974.
(3) Ge, C.M.; Zhang, S.H.; Feng, C.Y.; Wang, G.; Li, W.Z. *Anorg. Allg. Chem.* **2011**, *637*, 112–116.
(4) Zou, H.H.; He, Y.P.; Gui, L.C.; Liang, F.P. *CrystEngComm.* **2011**, *13*, 3325–3329.
(5) Fortin, S.; Beauchamp, A.L. *Inorg. Chem.* **2001**, *40*, 105–112.
(6) Yang, Y.; Tan, M.X.; Li, X.; Chen, X.M.; Tan, A.Z.; Qin, R.H.; Duan, W.G. *Chin J. Struct. Chem.* **2010**, *29*, 1900–1903.
(7) Yang, Y.; Yan, L.T.; Li, X.; Chen, X.M.; Qin, R.H.; Duan, W.G.Z. *Naturforsch* **2011**, *66b*, 889–893.
(8) Ren, H.; Song, T.Y.; Xu, J.N.; Jing, S.B.; Yu, Y.; Zhang, P.; Zhang, L.R. *Cryst. Growth Des.* **2009**, *9*, 105–112.
(9) Yang, Y.; Tan, M.X.; Li, X.; Chen, X.M.; Chen, G.Q.; Qin, R.H.; Duan, W.G. *J. Mol. Struct.* **2010**, *975*, 372–375.
(10) Escande, A.; Guénée, L.; Buchwalder, K.L.; Piguet, C. *Inorg. Chem.* **2009**, *48*, 1132–1147.
(11) Tadokoro, M.; Nakasuji, K. *Coord. Chem. Rev.* **2000**, *198*, 205–218.
(12) Lemos, S.S.; Deflon, V.M.; Bessler, K.E.; Abbott, P.M.; Niquet, E. *Transition Met. Chem.* **2004**, *29*, 46–50.
(13) Walsh, P.D.; Clérac, R.; Hearns, G.R.N.; Krugerd, E.P.; Schmitt, W. *CrystEngComm* **2009**, *11*, 1666–1673.
(14) Dai, F.N.; He, H.Y.; Gao, D.L.; Ye, F.; Sun, D.F.; Pang, Z.J.; Zhang, L.; Dong, G.L.; Zhang, C.Q. *Inorg. Chim. Acta.* **2009**, *362*, 3987–3992.
(15) Xu, Y.Q.; Yuan, D.Q.; Wu, B.L.; Han, L.; Wu, M.Y.; Jiang, F.L.; Hong, M.C. *Cryst. Growth Des.* **2006**, *6*, 1168–1174.
(16) Kongshaug, O.K.; Fjellvåg, H. *Inorg. Chem.* **2006**, *45*, 2424–2429.
(17) Wu, C.D.; Lu, C.Z.; Yang, W.B.; Zhuang, H.H.; Huang, J.S. *Inorg. Chem.* **2002**, *41*, 3302–3307.
(18) Yang, Y.; Zeng, M.H.; Zhang, L.J.; Liang, H. *Chin J. Struct. Chem.* **2009**, *28*, 1671–1676.
(19) Yang, Y.; Zeng, M.H.; Zhang, L.J.; Liang, H. *J. Coord. Chem.* **2009**, *62*, 886–893.
(20) Yang, Y.; Zeng, M.H.; Zhao, X.H.; Liang, H. *Inorg. Chim. Acta.* **2009**, *362*, 3065–3068.
(21) Marmur, J. *J. Mol. Biol.* **1961**, *3*, 208–218.
(22) Reichmann, E.M.; Rice, S.A.; Thomas, C.A.; Doty, P. *J. Am. Chem. Soc.* **1954**, *76*, 3047–3053.
(23) Sheldrick, G.M. *SHELXS-97, Program for Crystal Structure Determination*; University of Göttingen: Göttingen, Germany, 1997.

(24) Sheldrick, G.M. *SHELXL-97, Program for Crystal Structure Refinement*; University of Göttingen: Göttingen, Germany, 1997.
(25) Nishida, Y.; Tanaka, N.; Yamazaki, A.; Tokii, T.; Hashimoto, N.; Ide, K.; Iwasawa, K. *Inorg. Chem.* **1995**, *34*, 3616–3620.
(26) Matthews, J.C.; Leese, A.T.; Clegg, W.; Elsegood, R.J.M.; Horsburgh, L.; Lockhart, C.J. *Inorg. Chem.* **1996**, *35*, 7563–7571.
(27) Matthews, J.C.; Clegg, W.; Heath, L.S.; Martin, C.N.; Hill, M.N.S.; Lockhart, C.J. *Inorg. Chem.* **1998**, *37*, 199–207.
(28) Wu, S.S.; Zhang, Y.F.; Du, J.F.; Zhang, Q.; Yuan, W.B.; Gu, H.B. *Spectrosc. Spect. Anal.* **2008**, *28*, 374–379.
(29) Liu, J.; Zhang, T.X.; Lu, T.B.; Qu, L.H.; Zhou, H.; Zhang, Q.L.; Ji, L.N. *J. Inorg Biochem.* **2002**, *91*, 269–276.
(30) Tu, C.; Wu, X.F.; Liu, Q.; Wang, X.Y.; Xu, Q.; Guo, Z. *J. Inorg. Chim. Acta.* **2004**, *357*, 95–102.
(31) Ni, Y.; Lin, D.; Kokot, S. *Talanta* **2005**, *65*, 1295–1302.
(32) Thulstrup, P.W.; Thormann, Th.; Spanget-Larsen, J.; Bisgaard, H.C. *Biochem. Biophy. Res. Commun.* **1999**, *265*, 416–421.
(33) Barton, J.K.; Danishefsky, A.T.; Golderg, J.M. *J. Am. Chem. Soc.* **1984**, *106*, 2172–2176.
(34) He, X.Q.; Lin, Q.Y.; Hu, R.D.; Lu, X.H. *Spectrochim. Acta A* **2007**, *68*, 184–190.
(35) Harsh, R.H.; Barton, J.K. *J. Am. Chem. Soc.* **1992**, *114*, 5919–5925.
(36) Kumar, C.V.; Asuncion, E.H. *J. Am. Chem. Soc.* **1993**, *115*, 8547–8553.
(37) Claus, A.M.; Seidel, A.S.; Markus, H.M. *J. Phys. Chem.* **1996**, *100*, 5541–5553.
(38) Arounaguiry, A.; Bhaskar, M.G. *Inorg. Chem.* **2000**, *39*, 4256–4263.
(39) Liu, F.Q.; Wang, Q.X.; Jiao, K.; Jian, F.F.; Liu, G.Y.; Li, R.X. *Inorg. Chim. Acta.* **2006**, *359*, 1524–1530.
(40) Zhang, Q.L.; Liu, J.G.; Liu, J.Z.; Li, H.; Yang, Y.; Xu, H.; Chao, H.; Ji, L.N. *Inorg. Chim. Acta.* **2002**, *339*, 34–40.
(41) Raman, N.; Selvan, A. *J. Mol. Struct.* **2011**, *985*, 173–183.
(42) Goulle, V.; Harriman, A.; Lehn, J.M. *J. Chem. Soc. Chem. Commun.* **1993**, 1034–1036.
(43) Turro, C.; Bossman, S.H.; Jenkins, Y.; Barton, J.K.; Turro, N.J. *J. Am. Chem. Soc.* **1995**, *117*, 9026–9032.
(44) Dupureur, C.M.; Barton, J.K. *J. Am. Chem. Soc.* **1994**, *116*, 10286–10287.
(45) Friedman, A.E.; Kumar, C.V.; Turro, N.J.; Barton, J.K. *Nucleic Acids Res.* **1991**, *19*, 2595–2602.